Journal of Techniques, ISSN: 2708-8383, Vol. 6, No. 3, 2024, Pages 76-84
DOI: https://doi.org/10.51173/jt.v6i3.2598

JOURNAL OF TECHNIQUES

Journal homepage: http://journal.mtu.edu.iq

RESEARCH ARTICLE - ELECTRICAL AND ELECTRONIC ENGINEERING

An Efficiency Optimized Direct Model Predictive Control of Induction Machine Drive

Adeola Balogun[1], Sodiq Agoro[2], Sunday Adetona[1*], Ayobami Olajube[3], and Frank Okafor[1]

[1]Department of Electrical and Electronics Engineering, University of Lagos, Akoka, Nigeria

[2]Corporate Research Center, ABB Inc., Raleigh, North Carolina, USA

[3]Department of Electrical and Computer Engineering, Florida State University, Tallahassee, Florida, USA

[*] Corresponding author E-mail: sadetona@unilag.edu.ng

Article Info.

Article history:

Received
19 June 2024

Accepted
29 August 2024

Publishing
30 September 2024

Abstract

Presented in this paper is a direct model predictive control (MPC) for directly controlling the rotor speed and flux of an inverter-fed induction motor, which is also applicable to induction generators. Discrete dynamic model of the induction machine is applied in stationary reference frame with pre-set present and past reference values of the speed and rotor flux for generating the stator current references The uniqueness of the MPC proposed herein is that it does not require outer cascade proportional plus integral (PI) controllers used for regulating rotor speed and flux. Elimination of the outer loop cascade is made possible in this article by the introduction of a unique four-term cost function comprising of weighted magnitudes of the errors between four measured state variables and their reference commands. The four state variables in the unique cost function are the rotor speed, the rotor flux linkage, quadrature axis and direct axis stator currents. The MPC minimizes the cost function at every switching instance by selecting the switching states that gives the least cost function. Consequently, the selected optimal switching states are used to switch optimal inverter output voltages across the machine's stator terminals. As a precursor for obtaining an optimal rotor flux command in the MPC for every torque output, another unique efficiency improvement scheme is developed, which uniquely determines the stator angular velocity and the rotor flux that minimizes the core and copper losses while maintaining a constant slip operation. Therefore, efficacy of the proposed direct model predictive control scheme is verified by comparing its results to results obtained from equivalent vector control on equivalent machine. Results presented show lower loss regime with MPC on optimal stator angular velocity and rotor flux than vector control.

Publisher: Middle Technical University

Keywords: Induction Machines; PI Controller; Direct Model Predictive Control; Cost Function Minimization; State Variables.

1. Introduction

In the control of induction motors (IM), model based predictive schemes have in recent times become attractive and effective alternative to the conventional vector control and direct scalar control methods [1]. It has also been applied to the control of grid connected power converters; and has been shown to offer good results and performance [2]. In all of these, the future state of the system to be controlled is predicted in a defined horizon. A finite control set of voltage vectors are then used to minimize a cost function which reduces the difference between set references and the predicted values. In [3], model predictive flux control of IM drives was investigated. A proportional plus integral (PI) control cascade structure with switching instant optimization was used to reduce the torque ripple and current harmonics. Different methods in [4] and [5] have also been studied for the predictive speed control of IMs. These methods also have outer speed regulator; which is used for generating the reference torque or current required by the IM. In [6], a direct model predictive control (MPC) scheme was proposed whereby the need for a PI control cascade was eliminated. Therefore, the MPC was cascade-free, and all the state variables were used to formulate the cost function. However, the cascade-free MPC was utilized only for control of inverter based solar photovoltaic power evacuation into grid.

MPC schemes have also been applied to control other electric machines; for instance, in [7-12], different variants of MPC schemes were proposed for permanent magnet synchronous motors. In [8], a non-cascaded model-free predictive control was presented for control of surface magnet permanent magnet synchronous machine. In this case direct control of rotor speed was achieved by a cost function; which was formulated using the error between the reference rotor speed and actual rotor speed only. Errors in the quadrature and direct stator currents with their respective references were not used in the cost function formulation. However, constraints were placed on the quadrature and direct stator currents not to exceed their limits. In [9], the non-cascaded MPC in [8] was extended whereby the cost functions were formed using the summation of weighted square of errors in the rotor speed, the quadrature and direct stator currents and their respective references. Maximum torque per ampere was achieved via the MPC. However, neither the rotor flux nor the stator flux was regulated.

Nomenclature & Symbols			
q- d	Quadrature-Direct	v_{qs}, v_{ds}, v_q	*q*, *d*, and Complex *qd* Stator Voltages
i_{qs}, i_{ds}, i_{qds}	*q*, *d*, and Complex *qd* Stator Currents	λ_{qs}, λ_{ds}, λ_q	*q*, *d*, and Complex *qd* Stator Flux Linkages
i'_{qs},i'_{ds},i'_{qds}	*q*, *d*, and Complex *qd* Stator Currents	λ_{ss}	Square of Magnitude of Stator Flux Linkage
v_{qr}, v_{dr}, v_{qdr}	*q*, *d*, and Complex *qd* Stator Referred Rotor Voltages	L, L_r	Stator and Stator Referred Rotor Self-Inductances
λ_{rr}	Square of Magnitude of Rotor Flux Linkage	L_m	Inductance (3/2 in value)
r_s, r_r	Stator and Stator Referred Rotor Resistance	r_s, r_r	Stator and stator Referred Rotor Resistance
ω, ω_e	Angular velocity in Arbitrary, and Synchronous Frames	ω_r , ω_s	Rotor Speed, Stator Angular Velocity
λ_{qr}, λ_{dr}, λ_{qdr}	*q*, *d*, and Complex *qd* Stator Referred Rotor Flux Linkages	MPC	Model Predictive Control
i_{cq}, i_{cd}, i_{cqd}	*q*, *d*, and Complex *qd* Core Loss Currents	PI	Proportional Plus Integral
i_{qr}, i_{dr}, i_{qdr}	*q*, *d*, and Complex *qd* Stator Referred Rotor Currents	IM	Induction Machine

In this paper, therefore, a direct MPC for the control of speed and rotor flux of the IM that is cascade-free is presented. The cost in the proposed MPC for IM encapsulates the summation of weighted rotor speed error, weighted rotor flux error, and un-weighted quadrature and direct stator currents errors. It also develops an optimization algorithm which is used for efficiency optimization by minimizing the core and copper losses in the IM.

2. Methodology

2.1. Dynamic IM model

An equivalent circuit of the IM is shown in Fig. 1, and it would be used for the analysis of the machine.

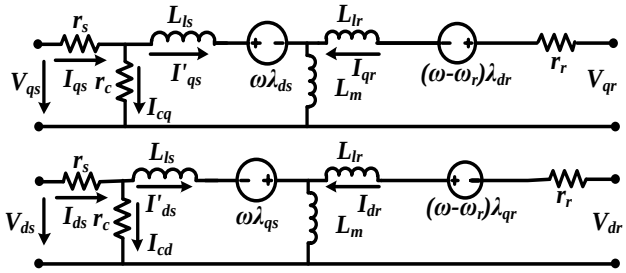

Fig. 1. *q–d* equivalent circuit model of induction machine including core–loss resistance

A state-space model of squirrel-cage IM developed from the conventional q-d reference vector variable model [13] is given in Eqs. (1-5).

$$L_o \frac{di_{qs}}{dt} = v_{qs} - ri_{qs} + r_r\lambda_{qr}\frac{L_m}{L_r^2} - \omega_r\lambda_{dr}\frac{L_m}{L_r} \tag{1}$$

$$L_o \frac{di_{ds}}{dt} = v_{ds} - ri_{ds} + r_r\lambda_{dr}\frac{L_m}{L_r^2} + \omega_r\lambda_{qr}\frac{L_m}{L_r} \tag{2}$$

$$\frac{d\lambda_{qr}}{dt} = -\frac{r_r}{L_r}\lambda_{qr} + \frac{r_r L_m}{L_r}i_{qs} + \omega_r\lambda_{dr} \tag{3}$$

$$\frac{d\lambda_{dr}}{dt} = -\frac{r_r}{L_r}\lambda_{dr} + \frac{r_r L_m}{L_r}i_{ds} - \omega_r\lambda_{qr} \tag{4}$$

$$\frac{d\omega_r}{dt} = \frac{P}{J}(T_e - T_m) \tag{5}$$

The electromagnetic torque T_e is given in Eq. (6).

$$T_e = (3PL_m/2L_r)(\lambda_{dr}i_{qs} - \lambda_{qr}i_{ds}) \tag{6}$$

The model is in the stationary reference frame when $\omega = 0$ and is used for developing a direct MPC scheme.

2.2. Steady-state IM model

The core loss in the machine is accounted for by resistance r_c. Therefore, the steady state stator and rotor voltage equations of IM in the arbitrary reference frame are given in Eq. (7) and Eq. (8) with all the differential terms set to zero.

$$V_{qds} = r_s I'_{qds} - j\omega_e\mu\lambda_{dqs} \tag{7}$$

$$V_{qdr} = r_r I_{qdr} - j(\omega_e - \omega_r)\lambda_{dqr} \tag{8}$$

Where $\lambda_{qds} = L_s I'_{qds} + L_m I_{qdr}$ (9)

$$\lambda_{qdr} = L_r I_{qdr} + L_m I'_{qds} \tag{10}$$

$$I_{qds} = I_{qdc} + I'_{qds} \tag{11}$$

$$\mu = 1 + r_s/r_c \tag{12}$$

In Eq. (11), I'_{qs} is the electromagnetic torque-producing stator current component.

2.3. Inverter model

The inverter-fed IM drive is illustrated in Fig. 2.

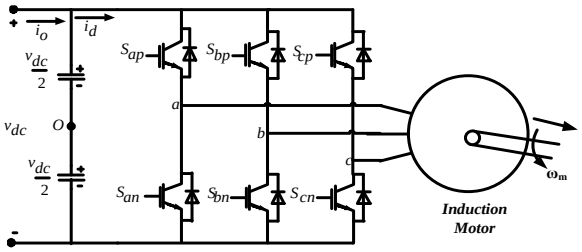

Fig. 2. An inverter-fed induction motor drive system

The stator terminals of the IM are fed from a 2-level three-phase voltage source inverter; whose output voltage quantities in stationary q-d reference frame are given in Eq. (13),

$$\begin{bmatrix} v_{qs} \\ v_{ds} \end{bmatrix} = \frac{v_{dc}}{3} \begin{bmatrix} 1 & -1/2 & -1/2 \\ 0 & \sqrt{3}/2 & -\sqrt{3}/2 \end{bmatrix} \begin{bmatrix} M_{ap} \\ M_{bp} \\ M_{cp} \end{bmatrix} \tag{13}$$

where each of M_{ap}, M_{bp}, and M_{cp} represents the modulation index for each of the phases. M_{ap}, M_{bp}, and M_{cp} are related to S_{ap}, S_{bp}, and S_{cp} respectively by $S_{ip} = 0.5(1 + M_{ip})$ i=a, b, c, which are the three-phase switching functions of the inverter's top leg (positive switching) power semiconductors. Each switching function taking a logic '1' or logic '0' state at every switching instance. The S_{ap}, S_{bp}, and S_{cp} are related to bottom-leg (negative) switching functions S_{an}, S_{bn}, and S_{cn} by $S_{ip} + S_{in} = 1$ where i=a, b, c, to guarantee that Kirchhoff's voltage law (KVL) is not violated by shorting the input DC voltage source.

2.4. Loss minimization

Eq. (14) gives the combined electrical losses of the core (iron) and copper losses (P_L) of the IM.

$$P_L = \frac{3}{2}\left(I_s{}^2 r_s + I_r{}^2 r_r + I_c{}^2 r_c\right) \tag{14}$$

In Eq. (14), the first two terms are the stator and rotor copper losses, while the last term yields the core loss. Fig. 3 (a) was obtained by keeping the rotor speed constant at 200 rad/s with a load torque of 3.8 Nm, and varying the stator angular velocity from 210 rad/s to 280 rad/s. In a variable frequency drive, under constant speed operation when the stator angular velocity increases with increase in rotor current, without saturation, the copper and core losses run contrarily as shown in Fig. 3(a), i.e. the copper loss increases while the core loss decreases. Therefore, the point of intersection of the core and copper losses create a compromise between the two losses which establishes a point of optimal operating regime. Therefore, the stator angular velocity and the rotor current at this point of intersection correspond to optimal values. The point of intersection will be determined subsequently.

In obtaining Fig. 3(b), the rotor speed was kept constant at 200 rad/s while the stator angular velocity was varied for each of the mechanical (load) torque values shown. Similar observation is noticed for other rotor speed values. It is easily seen in the figure that the minimal loss regimes for the three load torque values occur at the same stator angular velocity. In Fig. 3(c), there is a rotor flux linkage that corresponds with the minimal electrical losses. So, the question is: "Can the stator angular velocity and the rotor flux linkage that correspond to the minimal loss regime be uniquely determined?" Answer to this question will be given in the optimization procedure that will be given subsequently.

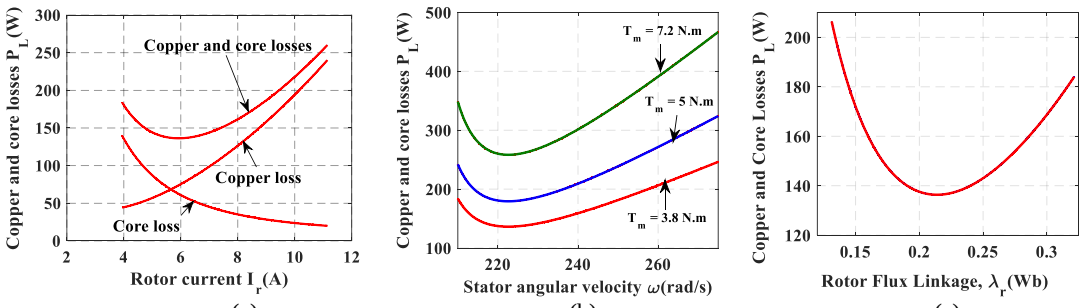

Fig. 3. (a) Copper and core losses versus rotor current; (b) Copper and core losses versus stator angular velocity; (c) Copper and core losses versus rotor flux linkage

The steady-state model given in sub-section 2.2 is used for loss minimization with an objective (cost) function of minimizing the stator copper, rotor copper, and core losses. Therefore, the real power loss equation in Eq. (14) and the electromagnetic torque in Eq. (6) are subjected to the classical Jacobi optimization procedure with respect to the stator angular velocity and magnitude of the rotor current. In Eq. (5), at steady-state the electromagnetic torque T_e equals the mechanical torque T_m. Consequently, with further substitution and simplification of Eq. (6), Eq. (15) is obtained for T_e, from which Eq. (16) is derived that is substituted in Eq. (14) to yield Eq. (17).

$$T_e = T_m = \frac{3P}{4}\left(\frac{r_r I_r^2}{(\omega-\omega_r)}\right) \tag{15}$$

$$I_r^2 = \frac{4(\omega-\omega_r)}{3Pr_r}T_e = \frac{4(\omega-\omega_r)}{3Pr_r}T_m \tag{16}$$

$$P_L = \left(a_{PL} + \frac{b_{PL}\omega}{(\omega-\omega_r)} + \frac{c_{PL}}{(\omega-\omega_r)^2}\right) I_r^2 \tag{17}$$

where, $a_{PL} = \frac{3}{2}\left[\frac{L_s}{L_m^2}(L_s^2(r_r - r_c) - r_r) - 2L_sL_r(r_r + r_c) + r_r + r_sL_m + L_m^2 r_c\right]$, and $b_{PL} = \frac{3r_r r_s}{2r_c}$, $c_{PL} = \frac{3}{2L_m^2}[r_s r_r^2(1 + L_s^2) + r_c L_s^2]$

Therefore, Eq. (18) is obtained as the Jacobi required for the loss minimization, which is subject to the constraints in Eq. (19). Consequently, an optimal stator angular velocity is obtained in Eq. (20).

$$\begin{vmatrix} \frac{dT_e}{dI_r} & \frac{dT_e}{d\omega} \\ \frac{dP_L}{dI_r} & \frac{dP_L}{d\omega} \end{vmatrix} = 0 \tag{18}$$

$$V_s = \sqrt{V_{qs}^2 + V_{ds}^2} \le V_{s\_rated} \text{ and } I_s = \sqrt{I_{qs}^2 + I_{ds}^2} \le I_{s\_rated} \tag{19}$$

$$\omega_{opt} = \omega_r \pm \sqrt{\frac{A_c}{B_c}} \tag{20}$$

where, $A_c = r_c r_r^2(1 + L_s^2) + r_c^2 r_r^2 L_s^2$, and $B_c = r_c r_s(1 + L_s^2)L_r^2 - 2r_c r_s L_s L_r L_m^2 + 2r_s r_r L_m^2 + r_c r_r L_m^2 + r_c^2 L_s^2 L_r^2 - 2r_c^2 L_s L_r L_m^2 + r_c^2 L_m^4$

An insight into Eq. (20) reveals that with the optimization procedure, the slip of the induction machine will always be kept constant at all rotor speed for minimization of electrical losses to be guaranteed. Aligning the rotor flux such that $\lambda_{qr}=0$ and $\lambda_{dr}=\lambda_r$, where $\lambda_{qr}^2 + \lambda_{dr}^2 = \lambda_r^2$, then from the d-axis component of Eq. (8) $I_{dr}=0$, which implies that $I_{qr} = I_r$ at steady-state where $I_{qr}^2 + I_{dr}^2 = I_r^2$. Consequently, the optimal rotor flux linkage is given in Eq. (21).

$$\lambda_{dr} = -\frac{r_r I_{qr}}{\omega_{opt}-\omega_r} \tag{21}$$

$$I_{qr} = \sqrt{\frac{4T_m(\omega_{opt}-\omega_r)}{3Pr_r}} \tag{22}$$

Eq. (22) is derived from Eq. (15) to further evaluate Eq. (21) as Eq. (23), which gives a reference command rotor flux linkage for the model predictive control scheme.

$$\boldsymbol{\lambda_{dr\_opt}} = \pm\sqrt{\frac{\boldsymbol{4T_m r_r}}{\boldsymbol{3P(\omega_{opt}-\omega_r)}}} \tag{23}$$

The T_m can always be determined by developing a mechanical torque observer. An example of such observer was given in [14]. Therefore, unique equations for the optimal stator angular velocity in Fig. 2 (b) and the rotor flux linkage in Fig. 2 (c) have been obtained in Eq. (20) and Eq. (23), respectively.

2.5. Direct MPC scheme

2.5.1. Discrete model of IM

In general, model predictive control schemes entail using discrete models of dynamic systems for predicting the control inputs that give the least predefined cost function or multi-objective functions. The state variable model given in Eqs. (1-4) is considered for discretization. However, Eq. (3) and Eq. (4) are used to obtain Eq. (24) for further simplification in the control scheme.

$$\frac{d\lambda_{rr}}{dt} = 2\left(-\frac{r_r}{L_r}\lambda_{rr} + \frac{\lambda_{qr} r_r L_m}{L_r} i_{qs} + \frac{\lambda_{dr} r_r L_m}{L_r} i_{ds}\right) \tag{24}$$

In Eq. (24), $\lambda_{rr} = \lambda_{qr}{}^2 + \lambda_{dr}{}^2$ (25)

Hence, using Euler's forward approximation formula, the discrete model of the IM currents, rotor flux magnitude, and rotor speed is obtained in Eqs. (26-29) respectively.

$$i_{qs}(k+1) = i_{qs}(k) + \frac{T_s}{L_o}\left(v_{qs}(k) - ri_{qs}(k) + \frac{r_r L_m \lambda_{qr}(k)}{L_r{}^2} - \frac{\omega_r(k) L_m \lambda_{dr}(k)}{L_r}\right) \tag{26}$$

$$i_{ds}(k+1) = i_{ds}(k) + \frac{T_s}{L_o}\left(v_{ds}(k) - ri_{ds}(k) + \frac{r_r L_m \lambda_{dr}(k)}{L_r{}^2} + \frac{\omega_r(k) L_m \lambda_{qr}(k)}{L_r}\right) \tag{27}$$

$$\lambda_{rr}(k+1) = \lambda_{rr}(k) + 2T_s\left(-\frac{r_r}{L_r}\lambda_{rr}(k) + \frac{\lambda_{qr}(k) r_r L_m i_{qs}(k)}{L_r} + \frac{\lambda_{dr}(k) r_r L_m i_{ds}(k)}{L_r} \right) \tag{28}$$

$$\omega_r(k+1) = \omega_r(k) + \frac{T_s P}{J}\left(K\left(\lambda_{dr}(k) i_{qs}(k) - \lambda_{qr}(k) i_{ds}(k)\right) - T_m(k) \right) \tag{29}$$

In Eqs. (26-29), (*k*) and (*k+1*) are used to denote the present and immediate future values of the variables at each step-size while T_s is the sampling time.

2.4.2. Predictive Model

In this sub-section, the predicted future state variable of the IM is obtained from Eqs. (26-29). The predicted q-d state variables of the stator currents in Eq. (26) and Eq. (27) are compacted in complex form of Eq. (30).

$$i_{qds}{}^{P}(k+1) = i_{qds}(k) + \frac{T_s}{L_o}\left(v_{qds}(k) - r i_{qds}(k) + \frac{r_r L_m \lambda_{qdr}(k)}{L_r{}^2} - j\frac{\omega_r(k) L_m \lambda_{dqr}(k)}{L_r} \right) \tag{30}$$

In the conventional vector control schemes, the current loops serve as the inner loop control, while the speed and flux loops usually serve as the outer control loops with a view to obtaining cascaded control structure. In this MPC scheme, however, the term *'direct MPC'* is used because no outer cascade PI controller is required as described in [4, 5]. Rather than the cascaded control structure with PI, the q-d components of Eq. (30) are used in Eq. (28) and Eq. (29) to obtain Eq. (31) and Eq. (32).

$$\lambda_{rr}{}^{P}(k+1) = \lambda_{rr}(k) + 2T_s\left(-\frac{r_r}{L_r}\lambda_{rr}(k) + \frac{\lambda_{qr}(k) r_r L_m i_{qs}{}^{P}(k+1)}{L_r} + \frac{\lambda_{dr}(k) r_r L_m i_{ds}{}^{P}(k+1)}{L_r} \right) \tag{31}$$

$$\omega_r{}^{P}(k+1) = \omega_r(k) + \frac{T_s P}{J}\left(\frac{3P}{2}\left(\lambda_{dr}(k) i^{P}{}_{q_s}(k+1) - \lambda_{qr}(k) i^{P}{}_{ds}(k+1) \right) - T_m(k) \right) \tag{32}$$

2.6. Cost function minimization

The four term cost function for the direct MPC is given in Eq. (33). The four terms are the magnitude of the speed error; magnitude of the square of the rotor flux linkage; magnitude of both q-d components of the stator current. The minimization of the cost function entails determining the finite switching state that corresponds to the least cost function at every immediate future iteration. Consequently, the switching state that corresponds to the least cost function is selected for switching the inverter at every immediate step size.

$$\zeta = \left(\Lambda_{\omega}\left| \omega_r^{*}(k+1) - \omega^{P}{}_r(k+1) \right| + \Lambda_{\lambda}\left| \lambda_{rr}^{*}(k+1) - \lambda_{rr}^{P}(k+1) \right| + \Lambda_i\left| i_{qs}^{*}(k+1) - i_{qs}^{P}(k+1) \right| + \Lambda_i\left| i_{ds}^{*}(k+1) - i_{ds}^{P}(k+1) \right| \right) \tag{33}$$

In Eq. (33) Λ_{ω}, Λ_{λ}, and Λ_i represent the weight factors, which are selected to aid the convergence of the iterative process. However, the weight factors of the speed and rotor flux are selected to be of different values from each other and different from that of the stator current because they all experience different dynamic states. In this case, speed and rotor flux regulation is the primary objective, hence Λ_{ω}, Λ_{λ} are chosen to be greater than $\Lambda_i = 1$. Furthermore, consideration is also given to compensate for the slow speed dynamics by specifically changing the iteration step of the speed in Eq. (33) to about *k+5* as given in Eq. (34). The variables with asterisks '*'in Eq. (33) and consequently Eq. (34) are the reference commands of the state variables.

$$\zeta = \left(\Lambda_{\omega}\left| \omega_r^{*}(k+5) - \omega^{P}{}_r(k+5) \right| + \Lambda_{\lambda}\left| \lambda_{rr}^{*}(k+1) - \lambda_{rr}^{P}(k+1) \right| + \Lambda_i\left| i_{qs}^{*}(k+1) - i_{qs}^{P}(k+1) \right| + \Lambda_i\left| i_{ds}^{*}(k+1) - i_{ds}^{P}(k+1) \right| \right) \tag{34}$$

2.7. Reference command variables

Unlike conventional vector control techniques that achieve decoupled control of the speed and rotor flux of an IM using cascaded PI control structure or predictive speed control methods that have an outer PI controller for speed regulation, the method proposed in this paper achieves the same control objectives without the use of linear speed regulators or a cascade PI structure. It uses the discrete dynamic model of the machine in Eq. (31) and Eq. (32) with the input reference values of speed and rotor flux in the previous and present sampling instant to obtain the reference q and d-axis currents of the machine. The future reference values of the stator currents, $i_{qs}{}^{*}(k+1)$ and $i_{ds}{}^{*}(k+1)$ given in Eq. (35) are thus obtained.

$$\begin{bmatrix} i_{qs}{}^{*}(k+1) \\ i_{ds}{}^{*}(k+1) \end{bmatrix} = \begin{bmatrix} \frac{KL_m\lambda_{dr}}{L_r} & \frac{-KL_m\lambda_{qr}}{L_r} \\ \frac{r_r L_m \lambda_{qr}}{L_r} & \frac{r_r L_m \lambda_{dr}}{L_r} \end{bmatrix}^{-1} \begin{bmatrix} \left(\frac{J(\omega^{*}{}_r(k) - \omega^{*}{}_r(k-1))}{PT_s} \right) + T_m \\ \left(\frac{\lambda_{rr}{}^{*}(k) - \lambda_{rr}{}^{*}(k-1)}{2T_s} \right) - \frac{r_r \lambda_{rr}}{L_r} \end{bmatrix} \tag{35}$$

The reference command of the speed of the IM, for example, when connected to a wind turbine to operate as a generator is set by appropriate maximum power point tracking algorithm, and when operated as a motor the reference command is set by the operator. The rotor reference flux can be obtained from the optimization procedure of Section 2.3. Using Lagrange's extrapolation formula, the future reference value of the rotor speed and rotor flux can be obtained from Eq. (36) and Eq. (37), respectively. The overall direct MPC scheme is illustrated in Fig. 4.

$$\omega^*_r(k+1) = 2\omega^*_r(k) - \omega^*_r(k-1) \quad (36)$$
$$\lambda^*_{rr}(k+1) = 2\lambda^*_{rr}(k) - \lambda^*_{rr}(k-1) \quad (37)$$

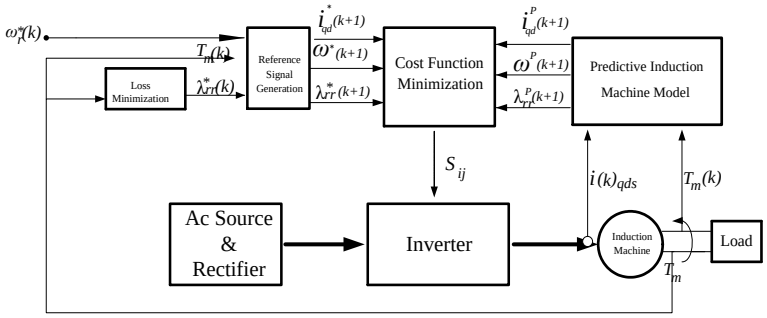

Fig. 4. Block diagram of the MPC scheme

3. Results and Discussions

Simulation of the proposed drive system was done in MATLAB/SIMULINK environment. The sampling time T_s for the MPC was selected as 10^{-5} s. The parameters of a 230–V line-line (rms), 60Hz, 4-pole squirrel–cage induction machine used in the simulation are given in Table 1.

Table 1. Machine Parameters

Parameter	Value
Stator resistance (rs)	0.435 Ω
Rotor referred resistance (rr)	0.816 Ω
Stator leakage inductance (Lls)	0.002 H
Rotor referred leakage inductance (Llr)	0.002 H
Magnetizing Inductance (Lm)	0.0693 H
Core loss resistance (rc)	850 Ω
Inertia (J)	0.089 kg.m^2

The simulation was done in two sets. In the first set, the load (mechanical) torque was set to 1 N.m and stepped to 0.5 N.m at 4 s, while the reference speed of the machine was set to ramp from zero at t=0 to 300 rad/s at t = 1 sec. At t = 2 s, a step change in speed from 300 rad/s to 250rad/s was set. Investigations on speed reversal operation of the IM was also set between t = 4 and t = 5 s. A step change in load disturbance was introduced to the system at t = 4 s. The reference of the square of the magnitude of the optimal rotor flux was computed from Eq. (23). Results obtained from the simulation are presented in Figs. 5 to 10.

In Fig. 5, the optimal stator angular velocity is shown, which was obtained from Eq. (20). The asymmetry in the pulse width of the switching functions in Fig. 6 implies the selection of the switching state that ensures that Eq. (34) is minimized at every instance of sampling. The waveform in Fig. 7 shows the actual IM rotor speed tracking the set references described. The difference between Figs. 5 & 7 maintains a constant slip. Fig. 8 shows the rotor flux magnitude tracking the optimal rotor flux reference set by the loss minimization scheme developed and follows the trajectory of the load torque. The rotor flux linkage follows the load torque profile of the induction motor, as can be seen in Fig. 8 that at 4 s when the load torque was stepped from 1 N.m to 0.5 N.m. the square of the magnitude of the rotor flux was also stepped down accordingly based on Eq. (4). Figs. 9 & 10 are the stationary q and d-axis stator currents of the IM respectively. In Figs. 9 & 10 both q and d stator currents reduced when the load torque was stepped from 1 N.m to 0.5 N.m. at 4 s.

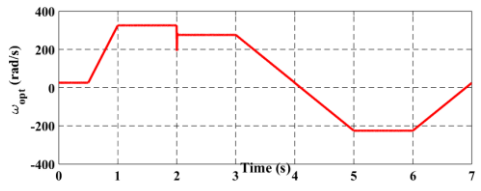

Fig. 5. Optimal stator angular velocity

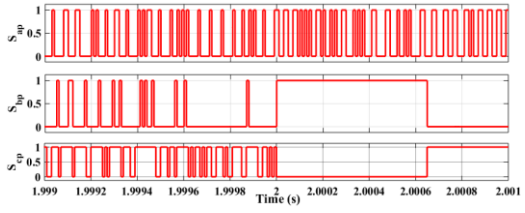

Fig. 6. Switching functions: S_{ap}. S_{bp}, and S_{cp}

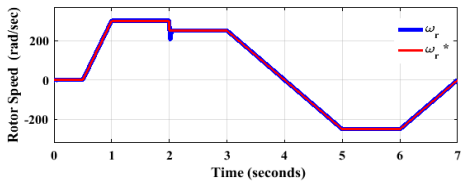

Fig. 7. Reference and actual rotor speed

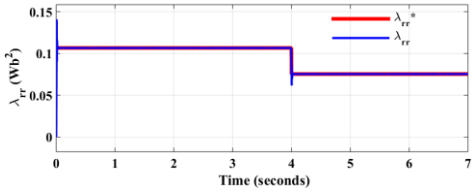

Fig. 8. Reference and actual square of magnitude of rotor flux linkage

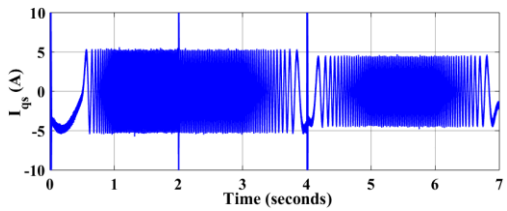

Fig. 9. Stator stationary q-axis current

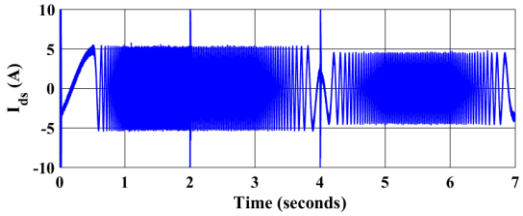

Fig. 10. Stator stationary d-axis current

In the second set of simulation, the load (mechanical) torque was set to 5 N.m while the rotor speed was fixed at 200 rad/s and the stator angular velocity was initially set at optimal value of 224 rad/s. The reason for these settings was to compare the stator and rotor currents with those obtained by setting the stator angular velocity at 210 rad/s, which is below optimal value, while the rotor speed was kept at 200 rad/s. Another reason was for comparing the stator and rotor currents from optimal setting with those obtained from induction machine on vector (rotor field orientation) control scheme with same machine parameters, load torque, rotor speed reference, and optimal stator angular velocity. The values of the stator and rotor currents give insight into the loss regime of the machine.

Therefore, Figs. 11 to 16 are results obtained from the MPC at the optimal settings. Figs. 11 and 12 show the rotor speed tracking the reference of 200 rad/s and the optimal rotor flux linkage was computed from Eq. (23), which gives the reference for the square of magnitude of rotor flux linkage (λ^*_{rr}) as 0.238 Wb^2. The stationary q and d stator currents are seen in Figs. 13 and 14, while the stationary rotor currents are seen in Figs. 15 and 16. Figs. 17 to 20 present the stationary q and d stator and rotor currents when the stator angular velocity was changed to 210 rad/s while keeping the rotor speed at 200 rad/s. When compared to Figs. 13 to 16, Figs. 17 to 20 are larger in magnitudes, with evidently more harmonics. As such, the loss regime from the operations at stator angular velocity changed to 210 rad/s remains higher than when at optimal value of 224 rad/s. Figs. 21 to 24 are the stationary q and d stator and rotor currents from equivalent vector control scheme on induction motor with stator angular velocity set at optimal 224 rad/s and optimal λ^*_{rr} obtained as 0.238 Wb^2. In comparative analysis, the stator and rotor currents from the MPC were lower in magnitudes than those obtained from the equivalent vector control scheme. Therefore, the loss regime of the vector control will be more than the MPC. The reason for such can be attributed to the minimization in MPC that selects switching functions set that correspond to minimal of Eq. (34). However, the switching of vector control is symmetrical but the switching of MPC is asymmetrical, which may yield slightly more ripples in the machine's electromagnetic torque from MPC.

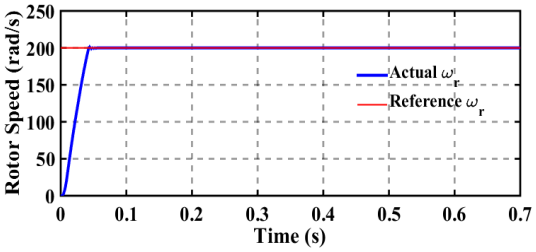

Fig.11. Reference and actual rotor speed

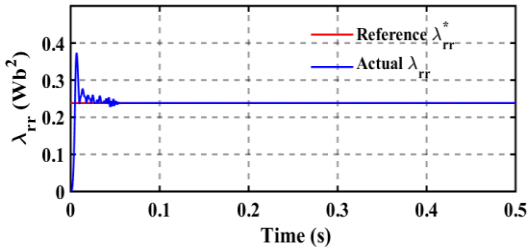

Fig. 12. Reference and actual square of magnitude of rotor flux linkage

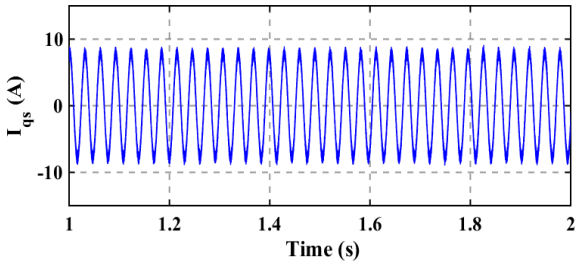

Fig. 13. Stator stationary q-axis current at optimal $\boldsymbol{\omega_{opt}} = \boldsymbol{224\ rad/s}$

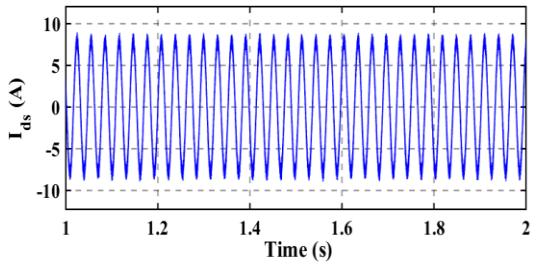

Fig. 14. Stator stationary d-axis current at optimal $\boldsymbol{\omega_{opt}} = \boldsymbol{224\ rad/s}$

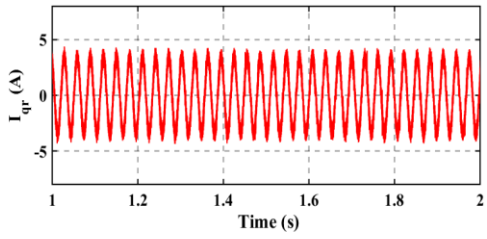

Fig. 15. Rotor stationary q-axis current at optimal $\boldsymbol{\omega_{opt}} = \boldsymbol{224\frac{rad}{s}}$

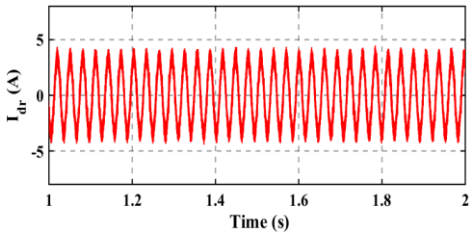

Fig. 16. Rotor stationary d-axis current at optimal $\boldsymbol{\omega_{opt}} = \boldsymbol{224\ rad/s}$

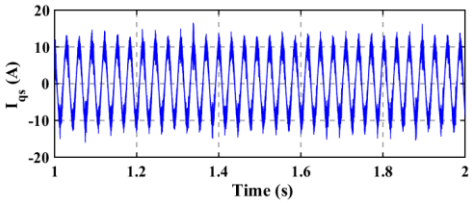

Fig. 17. Stator stationary q-axis current at $\boldsymbol{\omega_s = 210\ rad/s}$

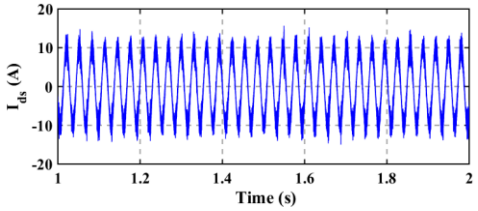

Fig. 18. Stator stationary d-axis current at $\boldsymbol{\omega_s = 210\ rad/s}$

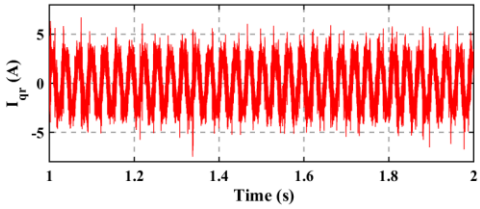

Fig. 19. Rotor stationary q-axis current at $\boldsymbol{\omega_s = 210\ rad/s}$

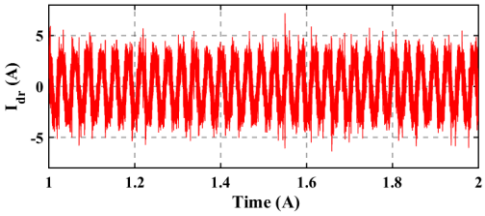

Fig. 20. Rotor stationary d-axis current at $\boldsymbol{\omega_s = 210\ rad/s}$

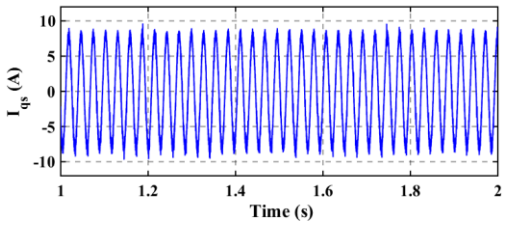

Fig. 21. Stator stationary q-axis current at optimal $\boldsymbol{\omega_{opt} = 224\ rad/s}$

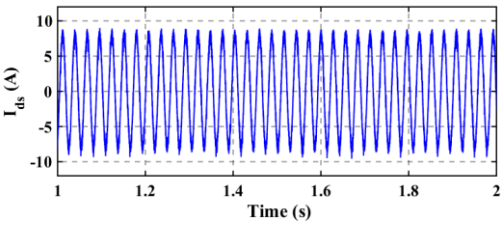

Fig. 22. Stator stationary d-axis current at optimal $\boldsymbol{\omega_{opt} = 224\frac{rad}{s}}$

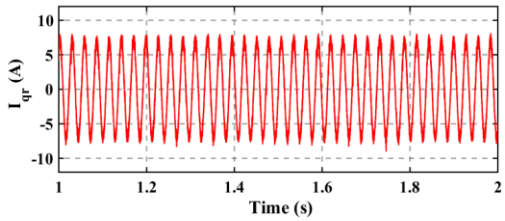

Fig. 23. Rotor stationary q-axis current at optimal $\boldsymbol{\omega_{opt} = 224\ rad/s}$

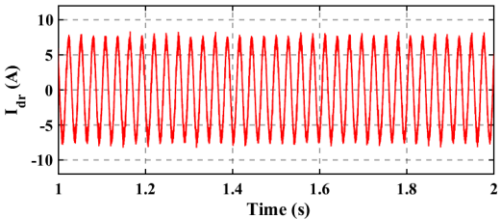

Fig. 24. Rotor stationary d-axis current at optimal $\boldsymbol{\omega_{opt} = 224\ rad/s}$

5. Conclusion

A PI controller-free model based predictive speed control scheme was developed for a squirrel cage IM in stationary reference frame. A four-term cost objective function consisting of different weight factors was used in selecting the switching states with the least errors. The efficiency improvement scheme developed uniquely computes the stator angular velocity and rotor flux linkage reference that minimized the core and copper losses while maintaining a constant slip operation. The results presented show effective performance of the proposed direct MPC scheme when step and ramp changes were introduced to the rotor speed and when step change was introduced to the load torque. Comparing the results obtained from MPC at optimal stator angular velocity and optimal rotor flux linkage to results from vector control yielded lower loss regime with the MPC. Therefore, the results presented show effective performance of the proposed direct MPC scheme.

Acknowledgment

I would like to express my appreciation to the Department of Electrical and Electronics Engineering, University of Lagos, for their support for the project requirements.

References

[1] C. A. Rojas, J. Rodriguez, F. Villarroel, J. R. Espinoza, C. A. Silva, and M.Trincado, "Predictive torque and flux control without weighting factors," IEEE Transaction on Industrial Electronics, vol. 60, no. 2, pp. 681–690, Feb. 2013. DOI: 10.1109/TIE.2012.2206344.

[2] P. Šimek, and V. Valouch, "Generalized predictive power control for grid-connected converter," International Journal of Electrical Power & Energy Systems, vol. 125, 106380, 2021. https://doi.org/10.1016/j.ijepes.2020.106380.

[3] Y. Zhang, and H. Yang, "Model-Predictive Flux Control of Induction Motor Drives with Switching Instant Optimization" IEEE Transactions on Energy Conversion, vol. 30, no. 3, September 2015. DOI: 10.1109/TEC.2015.2423692.

[4] E. Santana, E. Bim, and W. Amaral, "A Predictive Algorithm for Controlling Speed and Rotor Flux of Induction Motor" IEEE Transactions

On Industrial Electronics, vol. 55, no. 12, December 2008. DOI: 10.1109/TIE.2008.2007376.

[5] H. Miranda, P. Cortés, J. I. Yuz, and J. Rodríguez, "Predictive Torque Control of Induction Machines Based on State-Space Models" IEEE Transactions on Industrial Electronics, vol. 56, no. 6, June 2009 DOI: 10.1109/TIE.2009.2014904.

[6] S. Agoro, A. Balogun, O. Ojo and F. Okafor, "Direct Model-Based Predictive Control of a Three-Phase Grid Connected VSI for Photovoltaic Power Evacuation," 2018 9th IEEE International Symposium on Power Electronics for Distributed Generation Systems (PEDG), Charlotte, NC, USA, 2018, pp. 1-6, doi: 10.1109/PEDG.2018.8447817.

[7] Y. Zhou, H. Li , and H. Zhang. "Model-free deadbeat predictive current control of a surface-mounted permanent magnet synchronous motor drive system", Journal of Power Electronics. vol. 18, no 1, pp. 103-15. 2018 DOI: 10.6113/JPE.2018.18.1.103.

[8] J. Mao, H. Li, L. Yang, H. Zhang, L. Liu, X. Wang and J. Tao, "Non-cascaded model-free predictive speed control of SMPMSM drive system," IEEE Transactions on Energy Conversion, vol. 37, no. 1, pp. 153-162, 2021. DOI: 10.1109/TEC.2021.3090427.

[9] L. Yang, H. Li, J. Huang, Z. Zhang and H. Zhao, "Model predictive direct speed control with novel cost function for SMPMSM drives," IEEE Transactions on Power Electronics, vol. 37, no. 8, pp. 9586--9595, 2022. DOI: 10.1109/TPEL.2022.3155465

[10] M. Liu, K.W. Chan, J. Hu, W. Xu, and J. Rodriguez . "Model predictive direct speed control with torque oscillation reduction for PMSM drives", IEEE Transactions on Industrial Informatics, vol. 15, no. 9, pp. 4944-56. Feb. 2019 DOI: 10.1109/TII.2019.2898004.

[11] X. Zhang, Y. Cheng, Z. Zhao, and Y. He, "Robust model predictive direct speed control for SPMSM drives based on full parameter disturbances and load observer," IEEE Transactions on Power Electronics, vol. 35, no. 8, pp. 8361-73. Dec. 2019 DOI: 10.1109/TPEL.2019.2962857.

[12] C. Gong, Y. Hu, K. Ni, J. Liu and J. Gao, "SM Load Torque Observer-Based FCS-MPDSC With Single Prediction Horizon for High Dynamics of Surface-Mounted PMSM," in IEEE Transactions on Power Electronics, vol. 35, no. 1, pp. 20-24, Jan. 2020, doi: 10.1109/TPEL.2019.2929714.

[13] A. R. Munoz, T.A. Lipo, "Complex vector model of the squirrel-cage induction machine including instantaneous rotor bar currents," IEEE Transactions on Industry Applications, vol. 35, no. 6, pp. 1332 – 1340, Dec. 1999 DOI: 10.1109/28.806047.

[14] Y.A. Zorgani, Y. Koubaa, and M. Boussak, "MRAS state estimator for speed sensorless ISFOC induction motor drives with Luenberger load torque estimation," ISA transactions, 61, pp. 308-317. 2016 https://doi.org/10.1016/j.isatra.2015.12.015.